

A. Abdellah, M. Larbi, D. Toumi

Open circuit fault diagnosis for a five-level neutral point clamped inverter in a grid-connected photovoltaic system with hybrid energy storage system

Introduction. Recently, the number of high and medium voltage applications has increased dramatically. The connection between these different applications requires series-parallel combinations of power semiconductors. Multilevel converter topologies provide major advantages to these applications. In this paper, a grid-connected photovoltaic system with a hybrid energy storage system using a five-level neutral point clamped inverter is studied. Although the multilevel inverter has many advantages over the two-level inverter, it has a high probability of experiencing an open circuit fault. In this context, the five-level inverter has 24 controllable switches, one of which may experience an open circuit fault at any time. Therefore, it plays an important part in the reliability and robustness of the whole system. The **novelty** of this paper presents an approach to accurately detect the open circuit fault in all insulated gate bipolar transistors of a five-level neutral point clamped inverter in a photovoltaic power generation application with a hybrid energy storage system. **Purpose.** Before using fault-tolerant control to ensure service continuity, fault diagnosis techniques must first be used, which are the crucial phase of reliability. **Methods.** A detection method based on the maximum and minimum error values is proposed. These errors are calculated using the expected and measured line-to-line pole voltages. **Results.** The open circuit fault detection method is implemented using MATLAB/Simulink. Simulation results showed the accuracy of detecting the open circuit fault in all insulated gate bipolar transistors in a short time. Moreover, this method is adaptable to several applications and is also robust to transient regimes imposed by solar irradiation and load variations. References 26, table 3, figures 16.

Key words: photovoltaic, fault diagnosis, five-level neutral point clamped inverter, line-to-line pole voltages.

Вступ. Останнім часом різко зростає кількість застосувань високої та середньої напруги. З'єднання між цими різними використаннями вимагає послідовно-паралельних комбінацій силових напівпровідників. Топології багаторівневих перетворювачів надають цим додатком великі переваги. У цій статті вивчається фотоелектрична система, підключена до мережі, з гібридною системою зберігання енергії, яка використовує п'ятирівневий інвертор із фіксуванням нейтральної точки. Хоча багаторівневий інвертор має багато переваг, порівняно з дворівневим інвертором, він має високу ймовірність виникнення обриву кола. У зв'язку з цим п'ятирівневий інвертор має 24 керувані перемикачі, один з яких будь-якої миті може зіткнутися з обривом кола. Таким чином, він відіграє важливу роль у надійності та стійкості всієї системи. **Новизна** цієї статті являє собою підхід до точного виявлення несправності розімкненого кола у всіх біполярних транзисторах із ізольованим затвором п'ятирівневого інвертора з фіксуванням нейтральної точки у фотоелектричних додатках для вироблення електроенергії з гібридною системою зберігання енергії. **Мета.** Перш ніж використовувати відмовостійкий контроль для забезпечення безперервності обслуговування, необхідно спочатку використовувати методи діагностики несправностей, які є вирішальним етапом надійності. **Методи.** Запропоновано метод виявлення, заснований на максимальному та мінімальному значеннях помилок. Ці помилки розраховуються з використанням очікуваних та вимірних міжфазних напруг на полюсах. **Результати.** Метод виявлення обриву кола реалізовано з використанням MATLAB/Simulink. Результати моделювання показали точність виявлення обриву кола у всіх біполярних транзисторах із ізольованим затвором за короткий час. Більш того, цей метод адаптується до кількох застосувань, а також стійкий до перехідних режимів, викликаних сонячним випромінюванням та змінами навантаження. Бібл. 26, табл. 3, рис. 16.

Ключові слова: фотогальванічна система, діагностика несправностей, п'ятирівневий інвертор із зажимом нейтралі, лінійна напруга на полюсах.

1. Introduction. Photovoltaic (PV) system is increasingly important as it is easy to set up and requires low maintenance. Currently, the energy demand in the public domain has been fulfilled through the implementation of stand-alone, grid-connected and hybrid PV system configurations [1]. However, like other renewable energy sources, solar energy tends to be intermittent because it is influenced by meteorological conditions [2]. Hence, the Energy Storage System (ESS) is typically needed in renewable energy based microgrid system to serve as a buffer between production and load. In microgrid systems, the incoming and outgoing power of the ESS elements varies considerably depending on the instantaneous power production and load status [3]. These intermittent variations negatively impact ESS performance, reduce ESS life and increase the cost of battery replacement, as batteries are featured with high-energy density, but have low-power density, low charge/discharge rates and slow dynamic response. One way around these problems is to combine multiple types of energy storage elements to create a Hybrid Energy Storage System (HESS). Currently, batteries and supercapacitors (SCs) are the most popular choices for many systems because SCs have high-power densities, offer a long life cycle with high efficiency and fast charge/discharge response [4, 5].

The grid-connected PV system with a HESS was widely studied in the literature [6, 7]. Moreover, this

system must be equipped with an inverter that presents the connection between the generator and the AC side. The inverter, which is based on power semiconductors, including insulated gate bipolar transistors (IGBTs) and diodes, is one of the most vulnerable components, and therefore plays an important role in the reliability and robustness of the overall system. According to a study, 34 % of faults in power converters are related to power semiconductors and mainly to controllable switches, while diodes have a lower failure rate [8].

The multi-level Neutral Point Clamped (NPC) inverter is increasingly used in grid-connected PV systems because it has many advantages over two-level inverters, including lower harmonic distortion of the output voltage, the best choice for medium to high power and low switching loss [9, 10]. However, the high number of power switching devices increases the chance of failure. The most common power semiconductor failures are open circuit (OC), short circuit (SC), which can occur due to high thermal or electrical strain, wire disconnection or gate driver failure [11]. In most cases, a short-circuit fault results in an overcurrent, which is very destructive and can immediately damage the IGBTs. Therefore, protection against short-circuit faults is often achieved through hardware solutions. In addition, industrial gate drivers protect the system against short circuits [12]. However,

© A. Abdellah, M. Larbi, D. Toumi

when an OC fault occurs, the system continues to operate, but the line current and DC bus voltage fluctuate, which may result in a secondary fault in the power converter or other devices. One of the most important ways to boost system reliability is through fault-tolerant techniques. Currently, fault tolerance methods for inverters are mainly classified into two categories: software-based approaches without additional hardware and hardware-based approaches [13]. However, fault diagnosis is a crucial phase of service continuity, because without it, it is impossible to reconfigure the converter correctly [14].

Literature review. Fault diagnosis methods for multilevel converters are still not widely studied in the literature due to their more recent development than two-level converters. Moreover, the diagnostic methods validated for two-level converters are not directly applicable to multilevel converters due to their large number of power components. These methods are classified into two categories: voltage-based methods and current-based methods. For methods based on currents [15] proposes a method using the Average Current Park Vector for a three level NPC inverter. Although this method can detect the OC fault in two switches, the possibility of the failure of two IGBTs at the same time is rare. In [16], the authors contribute to the improvement of the previously mentioned study by accurately detecting the faulty switch. However, this study is only dedicated to AC drive applications. A study based on the extension theory method to locate faults in a three-level NPC inverter supplying an AC motor is proposed in [17]. The inputs used for this method are the frequency spectra of the line current waveforms. For an AC motor drive, the frequency spectra are different depending on the faulty switch. However, for a grid-connected system, it is impossible to detect the OC fault because the frequency spectrum is the same for the upper half arm as well as for the lower half arm. The authors of [18] accurately locate

the OC fault in a three-level NPC converter associated with a wind power system using the neural network. The inputs used in this study are the magnitude and phase angle of the generator currents. However, this method is limited to AC drive applications and requires large data storage and computing capacity.

For voltage-based methods, the authors of [19] propose a method based on the evaluation of pole voltages and motor line currents to detect the fault in a three-level NPC inverter. Although this method has the ability to detect multiple OC faults in all IGBTs and clamp diodes, it is not suitable for grid-connected systems. In [20] the authors contributed significantly to the accurate location of the faulty IGBT in a three-level NPC rectifier without adding additional hardware. The estimated voltage errors are represented by the expected value of the converter line voltage and its estimated value. However, this estimation generates a lot of noise, and the choice of thresholds and minimum detection time depends on each system, which reduces the robustness of this method. Fault detection of a five-level NPC inverter is not studied at all in the literature. The authors in [21] focused on the reconfiguration of this inverter without specifying the diagnostic method.

The goal of the paper. To remedy the previously mentioned drawbacks, this study presents an approach to accurately detect the OC fault in all IGBTs of a five-level NPC inverter. This inverter is used in a grid-connected PV system with a HESS to improve the power quality and to be able to support high power. The detection method is based on the maximum and minimum error values resulting from the comparison between the measured line-to-line pole voltages and their expected values. The fault monitoring is well achieved regardless of the load type (resistive or inductive) and power state (transient or steady-state), which amplifies the reliability of this algorithm. In addition, the proposed method can quickly detect the OC fault.

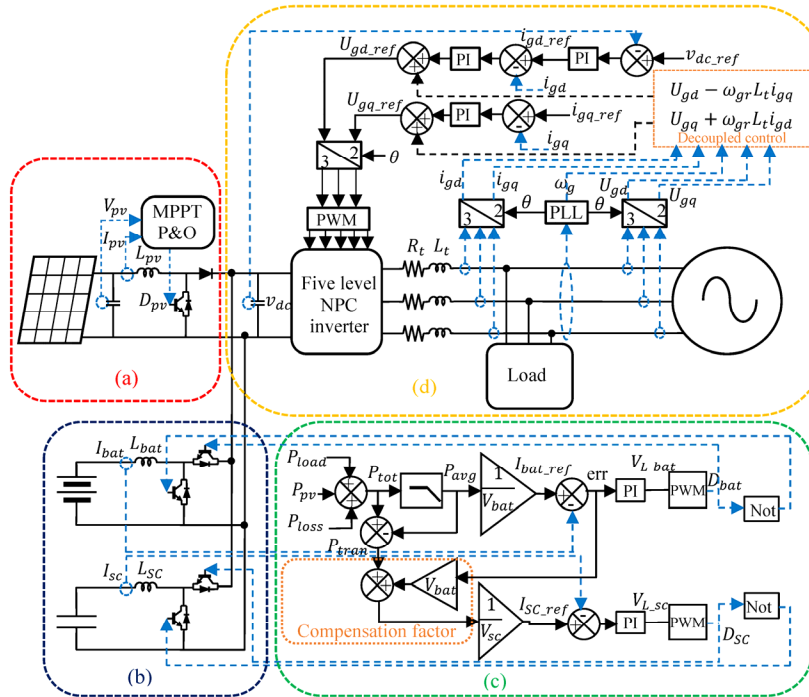


Fig. 1. Schematic diagram of grid-connected PV system with AC load

The Perturb & Observe method is used for extracting the maximum power of PV panels. It is an iterative method,

allowing acquiring the maximum power point. It depends on measuring the characteristics $I_{pv}(V_{pv})$ of the PV modules,

2. System description. The global system architecture is depicted in Fig. 1, which comprises three main functions: generation of electrical energy, HESS and energy management, connection to the grid.

2.1 PV generation. PV panels have been installed to produce electrical energy (Fig. 1,a). The PV generator is formed by PV panels connected in series for increasing the voltage and in parallel for increasing the current, and a DC/DC boost converter which transmits the produced power P_{pv} to the DC bus. The voltage V_{pv} at the terminals of the bank of panels, and the current I_{pv} passing through them, follow a $I_{pv}(V_{pv})$ characteristic which depends on the exogenous inputs which are the solar irradiation, and the atmospheric temperature. The electrical behavior of a PV cell can be described with good precision by a model called «single diode» [22].

then induces a slight disturbance of the voltage (or the current) to analyze the resulting power change [23].

2.2 Configuration of the HESS and energy management. Figure 1,*b* presents the HESS, which includes batteries and SCs. Each bank of SCs and batteries is connected to a DC/DC buck-boost converter, which connects it to the DC bus. There must be a complementarity between these hybrid storage systems. The batteries providing the «energy» function are sized in terms of average power, while the SCs having the «power» function are sized in transient power. The implementation of SCs is to improve battery life.

The energy management is presented in Fig. 1,*c*. To determine the total power P_{tot} , it is necessary to calculate the power of the PV generation P_{pv} , the power of the load P_{load} and the power dissipated in the grid filter P_{loss} . Then a low-pass filter is used to split the total power into two components: the transient power component P_{tran} and the average power component P_{avg} . Consequently, the part containing the high frequencies (transient power) is supplied to the SCs and those of the low frequencies to the batteries [24]. The power balance equation is stated as follows:

$$P_{tot} = P_{load} + P_{loss} - P_{pv} = P_{avg} + P_{tran} \quad (1)$$

Since the components P_{tran} and P_{avg} are based on a reference current on the DC bus side, two gains are used to estimate the reference currents on the SC side (I_{SCref}) and battery side (I_{batref}). The measured values of the SC and battery current (I_{SC} and I_{bat}) are taken in order to compare them with their reference values. In addition, a compensation factor is used to increase system performance by recovering uncompensated battery power due to its slow dynamics [25]. This uncompensated power is added to the transient power to be recovered by SC. Finally, the PI controllers are concerned with the generation of adequate control signals via the duty cycles of the converters (D_{SC} and D_{bat}), which allow the measured currents to follow their references.

2.3 Control of grid connection. The grid connection consists of a five-level NPC inverter, an $R-L$ filter at each phase, a load and a power grid as shown in Fig. 1,*d*. To control the grid side, Voltage Oriented Control (VOC) is proposed in this paper using the PI controller. The purpose of the VOC is to keep the DC bus voltage constant regardless of the amplitude and direction of the power. This control technique needs to calculate the angle using a phase locked loop for the Park transform. The control strategy comprises an outer loop to control the DC bus voltage and two internal loops to control the direct and quadrature components of the current (d -axis and q -axis). The external loop is then produced employing a regulation loop, making it possible to maintain a constant DC bus voltage, with a PI regulator generating the current reference I_{gdref} . Concerning the internal loop, the direct and quadrature components are used to regulate active and reactive power, respectively. Furthermore, a decoupled control for direct and quadrature components is implemented to tackle the problem of the relationship between the d -axis and q -axis [26].

3. Open circuit fault analysis. This section presents the analysis of the OC fault in a five-level NPC inverter, which is shown in Fig. 2 by the arm of the A phase. The five-level NPC inverter arm consists of four capacitors of equal capacity dividing the input voltage V_{dc} into four identical voltage levels and eight switches (IGBTs) mounted in antiparallel with diodes. In addition, six clamp

diodes are present to have five additional voltage levels, as shown in Table 1 [9].

This analysis is only dedicated to the switches of the upper half arm of phase A S_{A1} , S_{A2} , S_{A3} , S_{A4} due to its symmetrical shape. Therefore, the switches of the lower half arm S_{A5} , S_{A6} , S_{A7} , S_{A8} have the same analysis as those of the upper half arm, except for the path and the sign of the phase current.

3.1 Open circuit fault in S_{A1} . When the OC fault arises in the switch S_{A1} , then the current path is D_1 , S_{A2} , S_{A3} , S_{A4} and the switching state P_2 is impossible as shown in Fig. 3,*a*. Figure 4,*a* represents when an OC fault occurs in S_{A1} at the instant $t = 0.5$ s, from this instant a part of the positive phase current (I_{Ma}) flows. Furthermore, the diode D_1 is reverse biased due to the grid voltage, which is greater than the DC bus voltage $V_{dc}/4$. The control increases the amplitude of the currents of other phases (I_{Mb} and I_{Mc}) to balance the power.

3.2 Open circuit fault in S_{A2} . When the OC fault has appeared at the switch S_{A2} , the switching states P_2 and P_1 are impossible. Therefore, the current path of the faulty phase (I_{Ma}) is formed by D_2 , S_{A3} and S_{A4} as shown in Fig. 3,*b*. Then the diode D_1 , which blocks the majority of the positive phase current, is reverse biased. Therefore, the positive phase current is 0, as shown in Fig. 4,*b*.

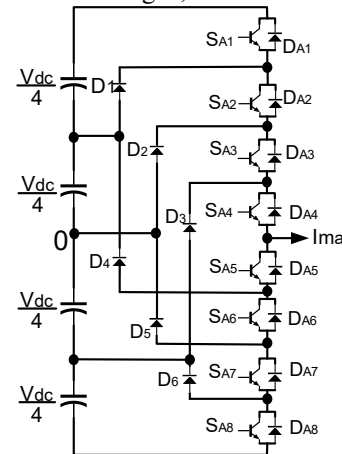


Fig. 2. The A -phase arm of a five-level NPC inverter

Table 1

State of leg X	IGBT's states $X \in \{A, B, C\}$								Pole voltage V_{XO}
	S_{X1}	S_{X2}	S_{X3}	S_{X4}	S_{X5}	S_{X6}	S_{X7}	S_{X8}	
P_2	1	1	1	1	0	0	0	0	$+V_{dc}/2$
P_1	0	1	1	1	0	0	0	0	$+V_{dc}/4$
0	0	0	1	1	1	1	0	0	0
N_1	0	0	0	1	1	1	1	0	$-V_{dc}/4$
N_2	0	0	0	0	1	1	1	1	$-V_{dc}/2$

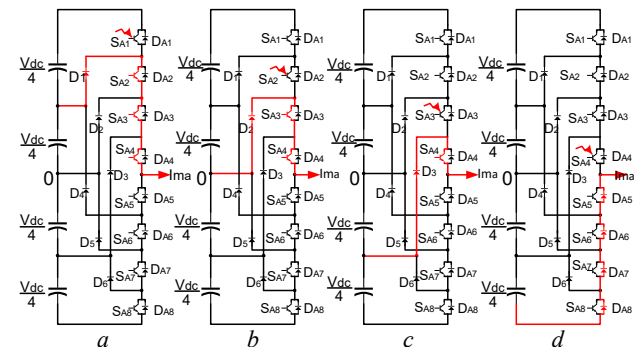


Fig. 3. Current paths in the case of an OC fault

3.3 Open circuit fault in S_{A3} . When S_{A3} is open-circuited, the impossible switching states are P_2, P_1 and 0. Therefore, the current path is formed by D_3, S_{A4} as shown in Fig. 3,c. However, because of the negative DC bus voltage and the positive grid voltage, diode D_3 is always reverse biased. So, the positive current corresponding to the faulty phase cannot flow, as shown in Fig. 4,c.

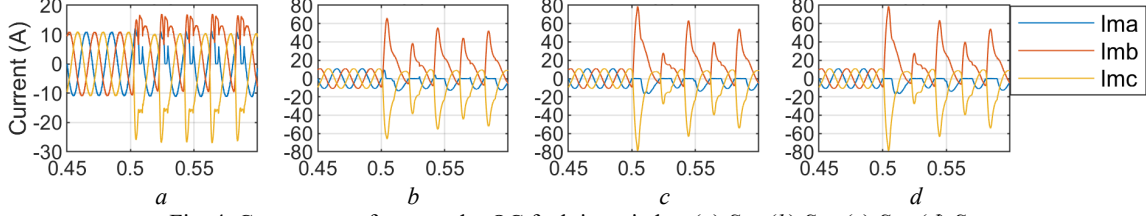


Fig. 4. Current waveforms under OC fault in switches (a) S_{A1} , (b) S_{A2} , (c) S_{A3} , (d) S_{A4}

From the previous analysis, the phase current is 0 in both situations when the switch S_{A3} or S_{A4} is faulty. The phase current when the fault occurs in S_{A5} or S_{A6} is also equal to each other. Therefore, if the load is not reactive, it is difficult or impossible to distinguish the OC fault from the switches mentioned above. Unless there are additional algorithms added to the detection technique. This will add a large computational capacity and slow down the detection time.

4. Diagnostic technique. In this section, a technique for detecting an OC fault of one of the switches of a five-level NPC inverter is proposed. This method is based on the comparison between the measured and expected line-to-line pole voltages, denoted V_{XY} and V_{XY}^* , respectively ($XY \in \{AB, BC, CA\}$). The five-level NPC inverter is controlled by the sine-triangle PWM control, which generates the control commands $\delta_{X_i} (i \in \{1, 2, \dots, 8\})$ to control the DC-bus voltage and the active and reactive power. Using these control commands those of the upper half arm of each phase, it is possible to estimate each pole voltage $V_{XO}^* (X \in \{A, B, C\})$ according to the following relation:

$$V_{XO}^* = (\delta_{X1} + \delta_{X2} + \delta_{X3} + \delta_{X4} - 2) \frac{V_{dc}}{2}. \quad (2)$$

The expected line-to-line pole voltages are:

$$V_{XY}^* = V_{XO}^* - V_{YO}^*. \quad (3)$$

To precisely locate the OC fault in each phase and each switch, the fault was analyzed using the deference between the expected and measured line-to-line pole voltages ΔV_{XY} . The diagnostic errors are calculated by:

$$\Delta V_{XY} = V_{XY}^* - V_{XY}. \quad (4)$$

The diagnostic errors must be normalized so that the diagnostic algorithm is independent of the DC bus voltage using the following formula:

$$\varepsilon_{XY} = \Delta V_{XY} / V_{dc}. \quad (5)$$

In healthy conditions, the diagnostic errors are 0, which means the measured and expected line-to-line pole are equal. On the other hand, if the OC fault has occurred in any switch, two-line voltage errors are affected by the OC fault, because each phase is linked to two line-to-line pole voltages. The third error, which has nothing to do with the faulty phase, remained 0.

Therefore, it is possible to accurately detect the defective half arm. For example, if the fault appeared in the upper half arm of phase X , the errors are as follows:

3.4 Open circuit fault in S_{A4} . When S_{A4} is open-circuited, the impossible switching states are $P_2, P_1, 0$ and N_1 . Therefore, the current path is formed by D_{A8}, D_{A7}, D_{A6} and D_{A5} as shown in Fig. 3,d. However, due to negative DC bus voltage and positive mains voltage, diode D_{A8}, D_{A7}, D_{A6} and D_{A5} are always reverse biased. So, the positive phase current cannot flow as shown in Fig. 4,d.

$$\begin{cases} \varepsilon_{XY} = \text{threshold}; \\ \varepsilon_{YZ} \approx 0; \\ \varepsilon_{ZX} = -\text{threshold}. \end{cases} \quad (6)$$

The diagnostic errors linked to defective phase X take symmetrical values. If the fault appeared in the lower half arm of phase X , the errors are the same, but the values of those linked to the defective phase are reversed.

After detecting the fault and determining the faulty phase and half-arm, it is necessary to identify with precision the faulty switch by determining the values of the errors corresponding to each switch. To calculate the maximum error value when S_{X1} is in OC, the current passes through D_1, S_{X2}, S_{X3} and S_{X4} instead as explained in section (3), connecting the DC bus mid-point (O) to the AC terminal and generating a pole voltage of value P_1 . This results in a pole voltage error ΔV_{XY} of $V_{dc}/4$. From (5), the normalized diagnostic error applied to the identification process (ε_{XY}) reaches a magnitude of 0.25 when the switching state is P_2 . Furthermore, the second normalized diagnostic error (ε_{ZX}) affected by the fault obtains a symmetrical value of -0.25 when the switching state is N_2 . The third error (ε_{YZ}), which is completely unrelated to the faulty phase, is 0. Using the analysis done in section (3), a similar process is employed to compute the normalized diagnostic error values for all switches, and the results are listed in Table 2.

However, these errors are not fixed at those values which vary at each cycle between 0 and the maximum value for the high error and between 0 and the minimum value for the low error. For this, it is only necessary to capture the maximum and minimum error values using an algorithm that calculates at any time the maximum and minimum error values, resulting in six errors $\{\max(\varepsilon_{XY}), \min(\varepsilon_{XY}), \max(\varepsilon_{YZ}), \min(\varepsilon_{YZ}), \max(\varepsilon_{ZX}), \min(\varepsilon_{ZX})\}$. Therefore, the fault detection of each switch relies on the behavior of these six errors and the threshold ranges in which these errors may exist. Table 3 summarizes the proposed OC fault detection method.

The diagnostic algorithm is recapitulated in the block diagram in Fig. 5. In summary, the algorithm begins with a step of calculating the expected pole voltages, and a line-to-line pole voltage measurement from which the necessary diagnostic errors are calculated. Then, as shown in Table 2, the maximum and minimum values of each normalized diagnostic error are extracted, since the errors don't have a

fixed value. An OC fault is recognized by checking (6), which identifies the faulty phase. In the event of a fault, the conditions in Table 3 immediately locate the faulty IGBT.

5. Simulation results and discussion. The simulation results of a grid-connected PV system with a hybrid storage system were performed via MATLAB. All the parameters of the studied system are presented in the Appendix. Power is injected via a balanced three-phase grid (220 V / 50 Hz). Before the system is subjected to an OC type fault, it is simulated in its healthy state to check the energy management. The PV generation power and the load power are shown in Fig. 6,a. From Fig. 6,b, it is evident that when the PV generation is higher than the demand the battery and the SC are charged by the difference of the two powers, and when the generation is lower than the load demand the

battery and the SC discharge to provide the rest of the required power. In the same figure, the SC supplies or absorbs the transient component of the current, while the battery supplies or absorbs the average component of the current. Figure 6,c shows the DC bus voltage following its reference (630 V). There are small fluctuations that are corrected by the PI regulator when the generation power or the load demand is changed. Figure 6,d illustrates the three-phase currents coming out of the five-level NPC inverter. The quality of the currents is very good thanks to this inverter. From Fig. 6,e, it is clear that the active power coming out of the inverter is the same as that of the load, which means that the energy management is working well. Since the load is purely active, the grid side controller maintains the reactive power around 0, as shown in Fig. 6,f.

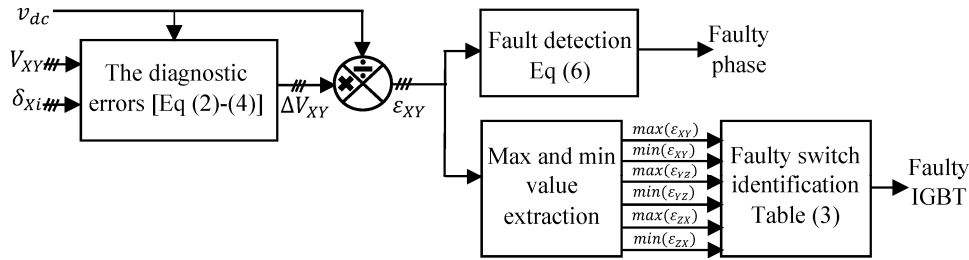


Fig. 5. Proposed diagnostic algorithm block diagram

Table 2

Normalized diagnostic errors with OC fault in phase X

Faulty switch	ϵ_{XY}					ϵ_{YZ}					ϵ_{ZX}				
	P_2	P_1	0	N_1	N_2	P_2	P_1	0	N_1	N_2	P_2	P_1	0	N_1	N_2
S_{X1}	0.25	0	0	0	0	0	0	0	0	0	0	0	0	0	-0.25
S_{X2}	0.5	0.25	0	0	0	0	0	0	0	0	0	0	0	-0.25	-0.5
S_{X3}	0.75	0.5	0.25	0	0	0	0	0	0	0	0	0	-0.25	-0.5	-0.75
S_{X4}	1	0.75	0.5	0.25	0	0	0	0	0	0	-0.25	-0.5	-0.75	-1	
S_{X5}	-1	-0.75	-0.5	-0.25	0	0	0	0	0	0	0.25	0.5	0.75	1	
S_{X6}	-0.75	-0.5	-0.25	0	0	0	0	0	0	0	0	0.25	0.5	0.75	
S_{X7}	-0.5	-0.25	0	0	0	0	0	0	0	0	0	0	0.25	0.5	
S_{X8}	-0.25	0	0	0	0	0	0	0	0	0	0	0	0	0.25	

Table 3

Look-up table for detection of the faulty IGBT of phase X

Faulty switch	$\max(\epsilon_{XY})$	$\min(\epsilon_{XY})$	$\max(\epsilon_{YZ})$	$\min(\epsilon_{YZ})$	$\max(\epsilon_{ZX})$	$\min(\epsilon_{ZX})$
S_{X1}	[0.05 0.25]	≈ 0	≈ 0	≈ 0	≈ 0	[-0.25 -0.05]
S_{X2}	[0.25 0.5]	≈ 0	≈ 0	≈ 0	≈ 0	[-0.5 -0.25]
S_{X3}	[0.5 0.75]	≈ 0	≈ 0	≈ 0	≈ 0	[-0.75 -0.5]
S_{X4}	[0.75 1]	≈ 0	≈ 0	≈ 0	≈ 0	[-1 -0.75]
S_{X5}	≈ 0	[-1 -0.75]	≈ 0	≈ 0	[0.75 1]	≈ 0
S_{X6}	≈ 0	[-0.75 -0.5]	≈ 0	≈ 0	[0.5 0.75]	≈ 0
S_{X7}	≈ 0	[-0.5 -0.25]	≈ 0	≈ 0	[0.25 0.5]	≈ 0
S_{X8}	≈ 0	[-0.25 -0.05]	≈ 0	≈ 0	[0.05 0.25]	≈ 0

To verify the effectiveness of the proposed detection technique, an OC type fault is imposed on the switches by forcing the switching states to 0. For the same parameters (irradiation and load) used previously, the OC type fault is generated at 0.55 s in switches S_{A3} , S_{B4} and S_{C7} , as shown in Fig. 7–9. From Fig. 7, the three fault cases show significant oscillations on the output currents of the faulty five-level NPC inverter. Consequently, the active power supplied to the load and the grid is no longer stable as well as the reactive power supplied to the grid is no longer equal to 0 and is oscillating, as shown in Fig. 8. Figure 9 shows a comparison between an ESS with and without SCs when the OC type fault occurs on the same switches mentioned previously. When the OC fault appeared, it turned out that

the SCs absorb the power peaks that are harmful to the batteries. These show small ripples as if nothing had happened. On the other hand, the system without hybrid storage (without SCs) forces the batteries to absorb the power peaks, which will reduce its lifespan.

The normalized diagnostic errors with which the fault can be detected are shown in Fig. 10. After $t = 0.55$ s, the behavior of these errors for the three fault cases is changed, which means that there is a fault. From Fig. 10,a, the ϵ_{AB} and ϵ_{CA} errors vary at 0.75 and -0.75 respectively, and ϵ_{BC} is around 0. From Table 2, the fault is in the S_{A3} switch. The fault can be easily detected using the same reasoning for Fig. 10,b,c. Furthermore, when the load changes at $t = 0.75$ s, these errors remain stable at maximum and minimum values.

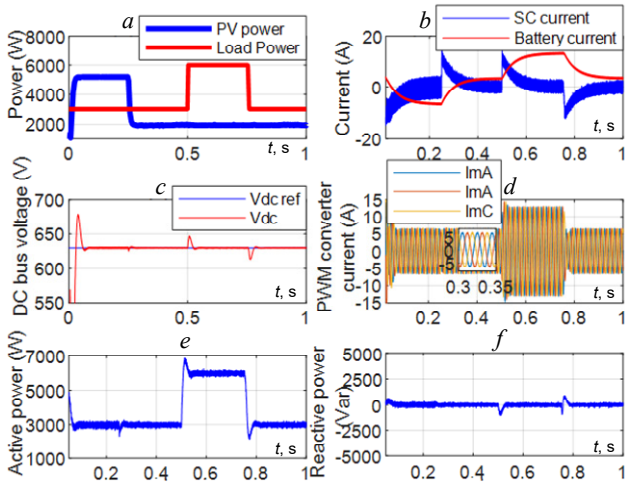


Fig. 6. The overall system behavior without OC fault

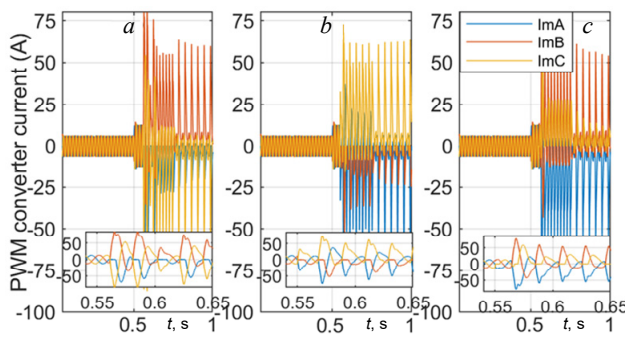


Fig. 7. The output currents of the PWM converter: a) OC fault in S_{A3} ; b) OC fault in S_{B4} ; c) OC fault in S_{C7}

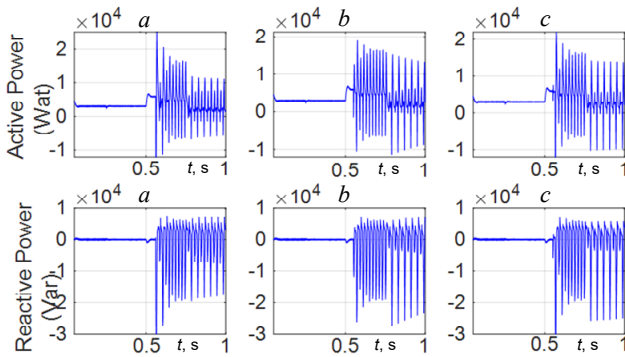


Fig. 8. Effects of an OC fault on active and reactive power: a) S_{A3} ; b) S_{B4} ; c) S_{C7}

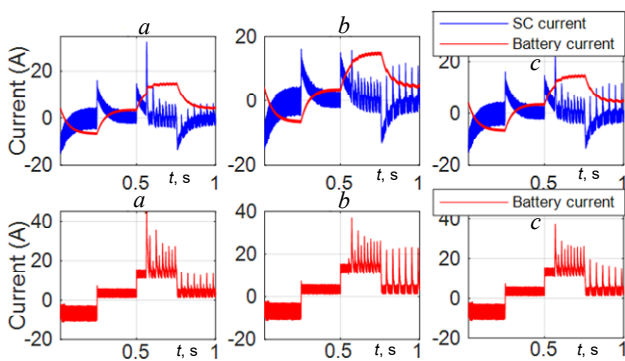


Fig. 9. Comparison between a storage system with and without SC under an OC fault: a) S_{A3} ; b) S_{B4} ; c) S_{C7}

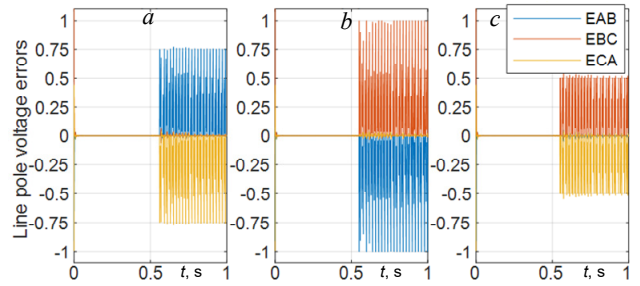


Fig. 10. Normalized diagnostic errors: a) S_{A3} ; b) S_{B4} ; c) S_{C7}

However, these errors switch between 0 and their maximum and minimum values. For this, Fig. 11 shows after using an algorithm to calculate the maximum and minimum point of each error. It is now easy to locate the fault using Table 3. The fault detection signals are presented in Fig. 12. Note that when the amplitude of the faulty phase detection signal is equal to «1» the fault is in phase A , «2» the fault is in phase B , and «3» the fault is in phase C . When the amplitude of the faulty switch detection signal is equal to «1» the fault is in switch S_{X1} , «2» the fault is in switch S_{X2} and so on, and «8» the fault is in switch S_{X8} . After the occurrence of an OC fault at 0.55 s in a five-level NPC inverter, the proposed method accurately detected it thanks to the six-normalized diagnostic errors. In addition, the time to identify each faulty switch is fast.

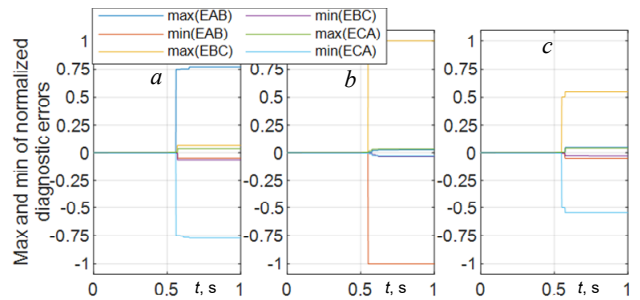


Fig. 11. Maximum and minimum values of the normalized diagnostic errors: a) S_{A3} ; b) S_{B4} ; c) S_{C7}

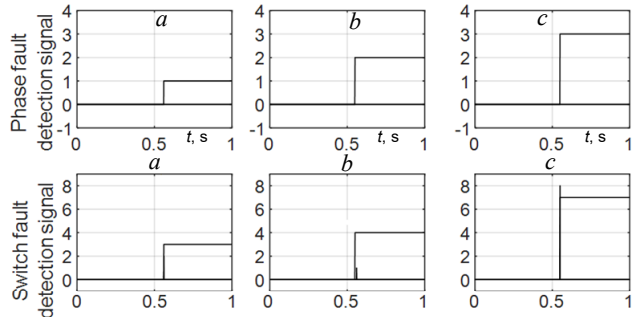


Fig. 12. Fault detection signals for phase and switch: a) S_{A3} ; b) S_{B4} ; c) S_{C7}

To test the robustness under transient conditions, the fault is shifted to $t = 0.5$ s which is the same time as the load variation. The OC fault is now applied to the switches S_{A5} , S_{B2} , S_{C3} . From Fig. 13, a-c, the maximum and minimum errors are the same values of Table 3 to detect the fault in switches S_{A5} , S_{B2} , S_{C3} . Therefore, the detection results are shown in Fig. 14, a-c. Moreover, for an active load fixed at a value of 2 kW with a reactive power of 2 kVAr, it is obvious that the OC fault is well detected, according to Fig. 15, 16.

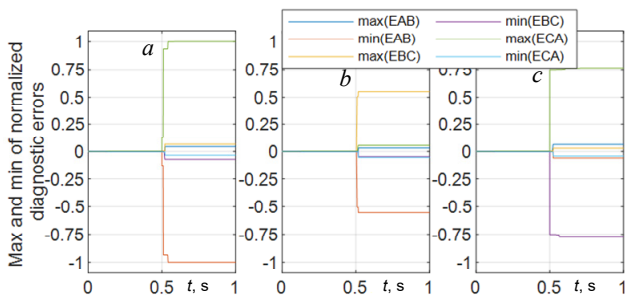


Fig. 13. Max and min values of the normalized diagnostic errors under transient conditions: a) S_{A5} ; b) S_{B2} ; c) S_{C3}

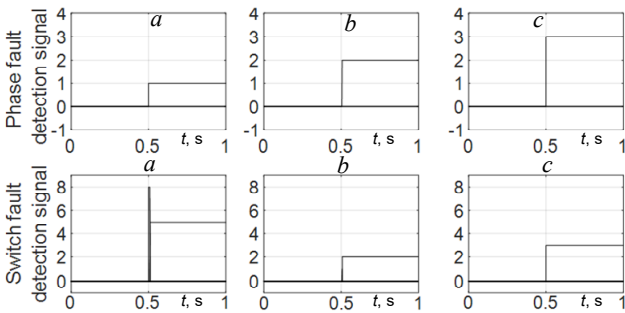


Fig. 14. Fault detection signals for phase and switch under transient conditions: a) S_{A5} ; b) S_{B2} ; c) S_{C3}

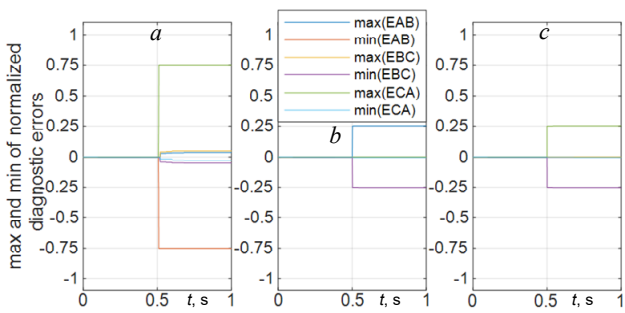


Fig. 15. Max and min values of the normalized diagnostic errors with active (2 kW) and reactive (2 kVAR) load: a) S_{A6} ; b) S_{B8} ; c) S_{C1}

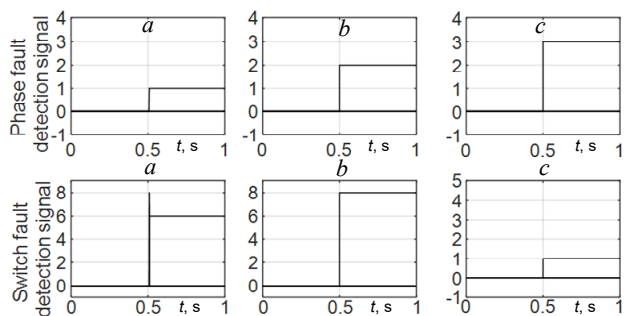


Fig. 16. Fault detection signals for phase and switch with active (2 kW) and reactive (2 kVAR) load: a) S_{A6} ; b) S_{B8} ; c) S_{C1}

6. Conclusions. A method for detecting an open circuit fault in a five-level neutral point clamped inverter has been proposed. This inverter has been used in a grid-connected photovoltaic system with a Hybrid Energy Storage System. The combination of the battery and supercapacitor improves the overall battery performance in terms of lifetime. Even when the open circuit fault occurs, the supercapacitor absorbs the ripples that are harmful to the battery. The detection method is mainly based on the calculation of the maximum and minimum point of each normalized diagnostic error, which results in six. These six

errors are determined by comparing the three measured line-to-line pole voltages with their expected values. The fault in each switch is related to the behavior of all six faults at once. Therefore, it is possible to discriminate the fault in each insulated-gate bipolar transistor through the lookup table. Furthermore, this method can identify the open circuit fault no matter what type of load. It is also robust to transient regimes imposed by solar irradiation and load variations, ensuring system reliability.

Appendix.

PV array parameters: MPPT power $P_m = 165$ W; inductor filter $L_{pv} = 10$ mH; cells in series $N_s = 8$; cells in parallel $N_p = 4$.

Battery parameters: terminal voltage $V_{bat} = 12$ V; inductor filter $L_{bat} = 8$ mH; A-h capacity 100 A-h; internal resistance 1.2 m Ω ; batteries in series – 25.

SC parameters: maximum voltage $V_{SC} = 2.5$ V; inductor filter $L_{SC} = 8$ mH; internal resistance 3.2 m Ω ; nominal capacity 350 F; SC in series – 120.

Utility grid parameters: DC bus capacitance $C = 900$ μ F; coupling inductance $L_f = 6.8$ mH; grid voltage $V_g = 380$ V; grid frequency $f = 50$ Hz.

Conflict of interest. The authors of the article declare that there is no conflict of interest.

REFERENCES

1. Cabrane Z., Kim J., Yoo K., Ouassaid M. HESS-based photovoltaic/batteries/supercapacitors: Energy management strategy and DC bus voltage stabilization. *Solar Energy*, 2021, vol. 216, pp. 551-563. doi: <https://doi.org/10.1016/j.solener.2021.01.048>.
2. Teleke S., Baran M.E., Bhattacharya S., Huang A.Q. Rule-Based Control of Battery Energy Storage for Dispatching Intermittent Renewable Sources. *IEEE Transactions on Sustainable Energy*, 2010, vol. 1, no. 3, pp. 117-124. doi: <https://doi.org/10.1109/TSTE.2010.2061880>.
3. Jing W., Hung Lai C., Wong S.H.W., Wong M.L.D. Battery-supercapacitor hybrid energy storage system in standalone DC microgrids: a review. *IET Renewable Power Generation*, 2017, vol. 11, no. 4, pp. 461-469. doi: <https://doi.org/10.1049/iet-rpg.2016.0500>.
4. Javed K., Ashfaq H., Singh R., Hussain S.M.S., Ustun T.S. Design and Performance Analysis of a Stand-alone PV System with Hybrid Energy Storage for Rural India. *Electronics*, 2019, vol. 8, no. 9, art. no. 952. doi: <https://doi.org/10.3390/electronics8090952>.
5. Khaligh A., Li Z. Battery, Ultracapacitor, Fuel Cell, and Hybrid Energy Storage Systems for Electric, Hybrid Electric, Fuel Cell, and Plug-In Hybrid Electric Vehicles: State of the Art. *IEEE Transactions on Vehicular Technology*, 2010, vol. 59, no. 6, pp. 2806-2814. doi: <https://doi.org/10.1109/TVT.2010.2047877>.
6. Roy P.K.S., Karayaka H.B., Yan Y., Alqudah Y. Investigations into best cost battery-supercapacitor hybrid energy storage system for a utility scale PV array. *Journal of Energy Storage*, 2019, vol. 22, pp. 50-59. doi: <https://doi.org/10.1016/j.est.2018.12.024>.
7. Kong L., Yu J., Cai G. Modeling, control and simulation of a photovoltaic /hydrogen/ supercapacitor hybrid power generation system for grid-connected applications. *International Journal of Hydrogen Energy*, 2019, vol. 44, no. 46, pp. 25129-25144. doi: <https://doi.org/10.1016/j.ijhydene.2019.05.097>.
8. Choi U.-M., Lee J.-S., Blaabjerg F., Lee K.-B. Open-Circuit Fault Diagnosis and Fault-Tolerant Control for a Grid-Connected NPC Inverter. *IEEE Transactions on Power Electronics*, 2016, vol. 31, no. 10, pp. 7234-7247. doi: <https://doi.org/10.1109/TPEL.2015.2510224>.
9. Himour K., Ghedamsi K., Berkouk E.M. Supervision and control of grid connected PV-Storage systems with the five level diode

- clamped inverter. *Energy Conversion and Management*, 2014, vol. 77, pp. 98-107. doi: <https://doi.org/10.1016/j.enconman.2013.09.001>.
10. Yang G., Fu C., Yi H., Chai C., Huang B., Hao S., Chen Z. Direct power control of three-level NPC grid-connected system combined with fault-tolerant technology. *Microelectronics Reliability*, 2018, vol. 88-90, pp. 1057-1062. doi: <https://doi.org/10.1016/j.microrel.2018.07.140>.
11. Jlassi L., Estima J.O., Khojet El Khil S., Mrabet Bellaaj N., Marques Cardoso A.J. Multiple Open-Circuit Faults Diagnosis in Back-to-Back Converters of PMSG Drives for Wind Turbine Systems. *IEEE Transactions on Power Electronics*, 2015, vol. 30, no. 5, pp. 2689-2702. doi: <https://doi.org/10.1109/TPEL.2014.2342506>.
12. Zhou D., Yang S., Tang Y. A Voltage-Based Open-Circuit Fault Detection and Isolation Approach for Modular Multilevel Converters With Model-Predictive Control. *IEEE Transactions on Power Electronics*, 2018, vol. 33, no. 11, pp. 9866-9874. doi: <https://doi.org/10.1109/TPEL.2018.2796584>.
13. Rehman H., Tariq M., Sarwar A., Alhosaini W., Hossain M.A., Batiyah S.M. Single-Phase Fault Tolerant Multilevel Inverter Topologies – Comprehensive Review and Novel Comparative Factors. *Energies*, 2022, vol. 15, no. 24, art. no. 9319. doi: <https://doi.org/10.3390/en15249319>.
14. Li H., Guo Y., Xia J., Li Z., Zhang X. Open-circuit fault diagnosis for a fault-tolerant three-level neutral-point-clamped STATCOM. *IET Power Electronics*, 2019, vol. 12, no. 4, pp. 810-816. doi: <https://doi.org/10.1049/iet-pel.2018.5802>.
15. Abadi M.B., Mendes A.M.S., Cruz S.M.A. Three-level NPC inverter fault diagnosis by the Average Current Park's Vector approach. *2012 XXth International Conference on Electrical Machines*, 2012, pp. 1893-1898. doi: <https://doi.org/10.1109/ICEIMach.2012.6350140>.
16. Mendes A.M.S., Abadi M.B., Cruz S.M.A. Fault diagnostic algorithm for three-level neutral point clamped AC motor drives, based on the average current Park's vector. *IET Power Electronics*, 2014, vol. 7, no. 5, pp. 1127-1137. doi: <https://doi.org/10.1049/iet-pel.2013.0416>.
17. Chao K.-H., Ke C.-H. Fault Diagnosis and Tolerant Control of Three-Level Neutral-Point Clamped Inverters in Motor Drives. *Energies*, 2020, vol. 13, no. 23, art. no. 6302. doi: <https://doi.org/10.3390/en13236302>.
18. Abid M., Larbi S., Larbi M., Allaoui T. Diagnosis and localization of fault for a neutral point clamped inverter in wind energy conversion system using artificial neural network technique. *Electrical Engineering & Electromechanics*, 2022, no. 5, pp. 55-59. doi: <https://doi.org/10.20998/2074-272X.2022.5.09>.
19. Abadi M.B., Mendes A.M.S., Cruz S.M.A. Method to diagnose open-circuit faults in active power switches and clamp-diodes of three-level neutral-point clamped inverters. *IET Electric Power Applications*, 2016, vol. 10, no. 7, pp. 623-632. doi: <https://doi.org/10.1049/iet-epa.2015.0644>.
20. Caseiro L.M.A., Mendes A.M.S. Real-Time IGBT Open-Circuit Fault Diagnosis in Three-Level Neutral-Point-Clamped Voltage-Source Rectifiers Based on Instant Voltage Error. *IEEE Transactions on Industrial Electronics*, 2015, vol. 62, no. 3, pp. 1669-1678. doi: <https://doi.org/10.1109/TIE.2014.2341558>.
21. Yu Y., Li X., Wei L. Fault Tolerant Control of Five-Level Inverter Based on Redundancy Space Vector Optimization and Topology Reconfiguration. *IEEE Access*, 2020, vol. 8, pp. 194342-194350. doi: <https://doi.org/10.1109/ACCESS.2020.3033805>.
22. Abdellah A., Toumi D., Larbi M., Moreau S. Zero-Compensator Filter for Power Sharing Between Battery/Supercapacitor in a Grid-Connected Photovoltaic System. *Advances in Electrical and Electronic Engineering*, 2022, vol. 20, no. 2, pp. 154-169. doi: <https://doi.org/10.15598/aee.v20i2.4321>.
23. Mostafa H.H., Ibrahim A.M., Anis W.R. A performance analysis of a hybrid golden section search methodology and a nature-inspired algorithm for MPPT in a solar PV system. *Archives of Electrical Engineering*, 2019, vol. 68, no. 3, pp. 611-627. doi: <https://doi.org/10.24425/aee.2019.129345>.
24. Jing W., Lai C.H., Wong W.S.H., Wong M.L.D. Dynamic power allocation of battery-supercapacitor hybrid energy storage for standalone PV microgrid applications. *Sustainable Energy Technologies and Assessments*, 2017, vol. 22, pp. 55-64. doi: <https://doi.org/10.1016/j.seta.2017.07.001>.
25. Manandhar U., Tummuru N.R., Kollimalla S.K., Ukil A., Beng G.H., Chaudhari K. Validation of Faster Joint Control Strategy for Battery- and Supercapacitor-Based Energy Storage System. *IEEE Transactions on Industrial Electronics*, 2018, vol. 65, no. 4, pp. 3286-3295. doi: <https://doi.org/10.1109/TIE.2017.2750622>.
26. Ali A.I.M., Mohamed H.R.A. Improved P&O MPPT algorithm with efficient open-circuit voltage estimation for two-stage grid-integrated PV system under realistic solar radiation. *International Journal of Electrical Power & Energy Systems*, 2022, vol. 137, art. no. 107805. doi: <https://doi.org/10.1016/j.ijepes.2021.107805>.

Received 24.11.2022
Accepted 03.03.2023
Published 02.11.2023

Abderrahmane Abdellah¹, PhD Student,
M'hamed Larbi¹, Full Professor,
Djilali Toumi¹, Senior Lecturer,
¹Department of Electrical Engineering,
L2GEGI Laboratory, University of Tiaaret, Algeria,
e-mail: abderrahmane.abdellah@univ-tiaaret.dz (Corresponding Author);
larbi_mh@yahoo.fr; toumi_dj@yahoo.fr

How to cite this article:

Abdellah A., Larbi M., Toumi D. Open circuit fault diagnosis for a five-level neutral point clamped inverter in a grid-connected photovoltaic system with hybrid energy storage system. *Electrical Engineering & Electromechanics*, 2023, no. 6, pp. 33-40. doi: <https://doi.org/10.20998/2074-272X.2023.6.06>